

When Gradient Clipping Becomes a Control Mechanism for Differential Privacy in Deep Learning

Mohammad Partohaghghi^a, Roummel Marcia^b, Bruce J. West^c, YangQuan Chen^{d,*}

^a*Electrical Engineering and Computer Science,
University of California, Merced, CA 95343, USA*

^b*Department of Applied Mathematics,
University of California, Merced, CA 95343, USA*

^c*Department of Innovation and Research,
North Carolina State University, Raleigh, NC, USA*

^d*Mechatronics, Embedded Systems and Automation (MESA) Lab,
Department of Mechanical Engineering, School of Engineering,
University of California, Merced, CA 95343, USA*

Abstract

Privacy-preserving training of neural networks for sensitive data analysis often relies on differentially private stochastic optimization with gradient clipping and noise injection. In this setting, the clipping threshold is a critical control knob: a small threshold can introduce substantial optimization bias through systematic over-clipping, while a large threshold can amplify the effect of injected noise and reduce predictive accuracy. Many adaptive clipping strategies attempt to tune this threshold using per-example gradient norm statistics, which can increase computational overhead and may be sensitive to dataset and architecture choices.

We propose a control-driven clipping strategy that regulates the clipping threshold using a lightweight, weight-only spectral diagnostic computed from model parameters. At periodic probe steps, the method analyzes a designated weight matrix through spectral decomposition and estimates a heavy-tailed spectral indicator that reflects training stability. This indicator is smoothed over time and fed into a bounded feedback controller that updates the clipping threshold multiplicatively in the log domain. Because the controller uses only model parameters produced during privacy-preserving training, the resulting updates constitute post-processing and do not increase privacy loss beyond that of the underlying privacy-preserving optimization mechanism under standard privacy accounting assumptions.

Across vision and tabular learning benchmarks under matched privacy budgets, the proposed approach improves utility and training stability relative to fixed-threshold clipping and remains competitive with representative adaptive clipping and privacy-preserving optimization baselines. Additional diagnostics and ablation analyses indicate stable controller behavior, robustness to reasonable probe and controller configurations, and modest computational overhead, with spectral probing accounting for only a small fraction of total training time.

Keywords: differential privacy, private deep learning, neural network training, gradient clipping, feedback control, heavy-tailed spectral analysis, sensitive data learning

*Corresponding author.

Email addresses: mpartohaghghi@ucmerced.edu (Mohammad Partohaghghi), rmarcia@ucmerced.edu (Roummel Marcia), brucejwest213@gmail.com (Bruce J. West), ychen53@ucmerced.edu (YangQuan Chen)

1. Introduction

Machine learning models are increasingly trained on sensitive data such as medical records, financial transactions, location traces, and user-generated content, where memorization and information leakage are not merely hypothetical failure modes but realistic adversarial objectives Partohaghghi et al. (2025). Differential Privacy (DP) provides a rigorous, composable guarantee that bounds what an observer can infer about any single individual from the released model or training outputs Dwork et al. (2006); Dwork & Roth (2014); Cheng et al. (2025); Yuan et al. (2021). For modern deep learning, the workhorse instantiation is *Differentially Private Stochastic Gradient Descent* (DP-SGD), which clips per-example gradients and injects Gaussian noise at each step Abadi et al. (2016). DP-SGD has enabled private training across diverse settings, but its practical performance is notoriously sensitive to one hyperparameter: the clipping threshold C .

The clipping bottleneck in DP-SGD. Clipping enforces a bound on per-example influence, making sensitivity finite and enabling calibrated Gaussian noise Abadi et al. (2016); Dwork & Roth (2014). Yet, C directly controls a three-way tension: (i) *clipping bias* (too small C truncates signal and underfits), (ii) *noise magnitude* (too large C increases the injected noise scale σC for a fixed noise multiplier σ), and (iii) *optimization stability* (interacting with learning rates, architecture, and loss geometry). A growing line of work has analyzed how clipping bias can dominate training dynamics and create failure modes even when privacy accounting is correct Chen et al. (2020); Xiao et al. (2023). In practice, practitioners often spend substantial compute sweeping C (and sometimes per-layer variants), which is expensive and frequently non-transferable across datasets, architectures, and training recipes.

Where the community has pushed: accounting, clipping, and optimizers. On the privacy side, DP-SGD’s guarantees rely on composition and amplification-by-subsampling analyses. Rényi Differential Privacy (RDP) Mironov (2017) and tighter subsampling accounting Wang et al. (2019); Balle et al. (2018) have become standard, while numerical and fast Fourier transform (FFT)-based accountants can yield tighter bounds for practical regimes Gopi et al. (2021); Ghazi et al. (2022). Alternative formalisms such as f -DP / Gaussian DP (GDP) offer a hypothesis-testing view and often simplify composition reasoning Dong et al. (2022). On the utility side, multiple approaches aim to reduce the brittleness of the clipping choice: coordinate-wise or adaptive clipping mechanisms Pichapati et al. (2019), private quantile/median-based adaptation in user-level settings Andrew et al. (2019), and more recent automatic clipping controllers for DP-SGD Bu et al. (2023a). A complementary direction improves DP training stability and convergence using (private) adaptive optimization, though adaptivity itself can be privacy-costly unless carefully engineered Li et al. (2023); Tang et al. (2024). Other work changes the sampling/training dynamics to improve signal-to-noise, for example importance sampling under DP constraints Wei et al. (2022) or sharpness-aware training adapted to DP to improve generalization under noise Foret et al. (2021); Park et al. (2023c). Finally, substantial engineering effort has gone into reducing DP-SGD overhead, especially per-example gradient computation and clipping Lee & Kifer (2021), and into mature software stacks for reproducible DP training Yousefpour et al. (2021); TensorFlow Privacy Authors (2019).

A spectral-control viewpoint. This paper introduces a different lens: treat clipping selection as a *closed-loop control* problem with a feedback signal that is (a) informative about training health and (b) safe under differential privacy post-processing. Our key observation is that deep networks’ weight matrices exhibit measurable spectral regularities that correlate with capacity, implicit regularization, and training phase. In particular, a line of

random-matrix-inspired work argues that well-trained networks often display *heavy-tailed* spectral structure and that fitted tail exponents can track model quality trends Martin & Mahoney (2021a, 2019, 2021b). The associated open-source *WeightWatcher* tool, a weight-spectrum analysis package inspired by random matrix theory, operationalizes this idea via spectral diagnostics computed directly from weights, without accessing training or test data at probe time Martin & Mahoney.

A weight-spectrum feedback controller for adaptive clipping under differential privacy. We propose **WW-DP-SGD**, a DP-SGD variant that adapts the clipping threshold C_t using a *weight-only* spectral health signal computed from the current (private) model parameters. At periodic probe steps, we estimate a WeightWatcher-style heavy-tailed exponent ζ_t from a chosen weight matrix and regulate training to keep ζ_t within a pre-defined *spectral health zone*. We use a saturated log-domain feedback law that continuously regulates toward the zone center, yielding stable two-sided updates in general and avoiding collapse of C_t . WW-DP-SGD does *not* claim additional privacy beyond DP-SGD. Under the same minibatching/subsampling assumptions and the same noise multiplier σ , privacy accounting follows the same established analyses used for DP-SGD Abadi et al. (2016); Mironov (2017); Wang et al. (2019); Gopi et al. (2021); Dong et al. (2022). The key point is that the spectral probe and the controller read only the current model parameters, which are outputs of a DP mechanism; therefore the adaptation of C_t is post-processing and cannot increase privacy loss Dwork & Roth (2014). Moreover, the per-step ℓ_2 sensitivity of the clipped gradient sum scales with C_t and the injected Gaussian noise scales with C_t as well, so the per-step privacy is governed by (q, σ) and composed over T steps by standard RDP/GDP accountants Mironov (2017); Dong et al. (2022).

Contributions. We summarize our main contributions as follows: **(Algorithmic)** we introduce **WW-DP-SGD**, a closed-loop DP-SGD variant that adaptively sets the clipping norm using a WeightWatcher-style spectral tail exponent together with a spectral “health zone” Martin & Mahoney (2021a); Martin & Mahoney; **(Control design)** we instantiate a log-domain saturated feedback controller with interpretable parameters (κ, β, r) and an optional experimental clamp (C_{\min}, C_{\max}) ; **(DP consistency)** we formalize why this controller preserves differential privacy under standard DP-SGD accounting assumptions via post-processing and composition Dwork & Roth (2014); Mironov (2017); Wang et al. (2019); **(Positioning vs. prior art)** we relate spectral feedback control to existing adaptive clipping and DP optimization methods Pichapati et al. (2019); Bu et al. (2023a); Wei et al. (2022); Li et al. (2023); Park et al. (2023c); and **(Practical guidance)** we provide implementation details such as probe-layer choice, probe period, smoothing, and controller gain along with evaluation protocols using common libraries for private training Yousefpour et al. (2021); TensorFlow Privacy Authors (2019); Lee & Kifer (2021).

Paper organization. Section 2 reviews DP-SGD and introduces the WeightWatcher-style spectral exponent used as a weight-only diagnostic signal. Section 3 presents WW-DP-SGD, including the log-domain saturated controller for adaptive clipping. Section 4 states the DP guarantee and the accounting protocol under Poisson subsampling. Section 5 evaluates privacy–utility trade-offs, robustness to clipping sensitivity and distribution shift, and runtime overhead. Section 6 discusses limitations and outlines directions for future work.

2. Background and Notation

We first define differential privacy (DP), then instantiate DP via DP-SGD under Poisson subsampling. Next, we introduce a *weight-only spectral diagnostic* (a WeightWatcher-style proxy derived from the weight spectrum) used as the feedback signal, and finally define the controller that adapts the clipping threshold while preserving DP guarantees through post-processing.

2.1. Differential Privacy

Definition 2.1 (Differential Privacy (DP)). Abadi et al. (2016) A randomized mechanism M is (ε, δ) -differentially private if for all neighboring datasets D, D' differing in exactly one example and all measurable sets S ,

$$\Pr[M(D) \in S] \leq e^\varepsilon \Pr[M(D') \in S] + \delta.$$

DP provides a worst-case stability guarantee: changing one training point has a limited effect on the distribution of the released output. We next review the standard training mechanism used in this work. Differentially Private Stochastic Gradient Descent (DP-SGD) is the standard way to train deep models under DP. Let $D = \{x_1, \dots, x_N\}$, parameters $\theta_t \in \mathbb{R}^d$, sampling rate $q \in (0, 1)$, and learning rate η_t . At step t , we independently include each example with probability q (Poisson subsampling), forming minibatch L_t . For each sampled example $x_i \in L_t$, compute the per-example gradient

$$g_t(x_i) = \nabla_{\theta} \mathcal{L}(\theta_t, x_i). \quad (1)$$

We initialize the clipping schedule with a user-specified $C_0 > 0$; in standard DP-SGD, $C_t \equiv C_0$ is fixed across steps, while in WW-DP-SGD C_t is adapted over time by the controller in Section 3.3. Clip to an ℓ_2 threshold $C_t > 0$,

$$\bar{g}_t(x_i) = \frac{g_t(x_i)}{\max\left(1, \frac{\|g_t(x_i)\|}{C_t}\right)}, \quad (2)$$

and add Gaussian noise calibrated to C_t . Writing I_d for the $d \times d$ identity matrix,

$$\tilde{g}_t = \frac{1}{|L_t|} \left(\sum_{x_i \in L_t} \bar{g}_t(x_i) + \mathcal{N}(0, \sigma^2 C_t^2 I_d) \right), \quad \theta_{t+1} = \theta_t - \eta_t \tilde{g}_t, \quad (3)$$

where σ is the noise multiplier (fixed across steps in our experiments). Under Poisson subsampling, $|L_t| = 0$ can occur. In that case, we perform a safe DP-preserving update by skipping the step (i.e., set $\theta_{t+1} = \theta_t$) and retaining C_t . This is post-processing and does not weaken DP. We compose privacy over T steps using either a Rényi Differential Privacy (RDP) accountant or a Privacy Loss Random Variable (PRV) accountant, both compatible with Poisson subsampling. The accountant takes (q, σ, T, δ) and returns (ε, δ) for the full run. The next ingredient is a weight-only spectral proxy that we use to adapt C_t in a controlled way.

3. The proposed algorithm

Overview.. This section presents WW-DP-SGD as a *DP-safe, closed-loop* variant of DP-SGD that adapts the clipping threshold without accessing per-example gradient statistics for control. We first define the weight-only diagnostic signal: a WeightWatcher-style estimate of a heavy-tailed spectral exponent ζ_t computed from a fixed probe weight matrix $W(\theta_t)$. We then introduce the notation used throughout the method and specify

a practical *spectral health zone* $(\zeta_{\min}, \zeta_{\max})$ that serves as the control target. Finally, we describe a log-domain saturated feedback controller that updates the clipping threshold C_t multiplicatively (with an optional clamp for numerical stability), and we summarize the full procedure in Algorithm 1.

3.1. WeightWatcher-style spectral exponent (WW)

To obtain a diagnostic signal from the model weights, we apply a WeightWatcher-style (WW) heavy-tail analysis to a fixed probe weight matrix $W(\theta_t) \in \mathbb{R}^{m \times n}$ (dense layers directly; convolutional kernels reshaped to 2D). Compute the singular value decomposition (SVD):

$$W(\theta_t) = U\Sigma V^\top, \quad \Sigma = \text{diag}(\sigma_1, \dots, \sigma_r), \quad (4)$$

and define eigenvalues $\lambda_j = \sigma_j^2$ of the correlation matrix $W^\top W$. We estimate a heavy-tailed exponent ζ_t by fitting a power-law to the *upper tail* of the spectrum:

$$p(\lambda) \propto \lambda^{-\zeta_t} \quad \text{for } \lambda \geq \lambda_{\min}. \quad (5)$$

In practice, the fit is performed on the largest eigenvalues (e.g., top- k or those exceeding a threshold) using robust regression in log-log coordinates. We denote this procedure as

$$\zeta_t = \text{WW}(W(\theta_t)).$$

In parts of the WW literature the exponent is often denoted by α ; here we use ζ consistently throughout the paper. This scalar proxy is then smoothed and fed to a controller that updates C_t multiplicatively in log-space.

3.2. Notation

Table 1: Notation used throughout the paper.

Symbol	Meaning
$D = \{x_i\}_{i=1}^N$	Dataset; N is dataset size
d	Parameter dimension ($\theta_t \in \mathbb{R}^d$)
q	Poisson subsampling rate
$t = 0, \dots, T - 1$	Step index; T total number of steps
C_0	Initial clipping threshold ($C_t \equiv C_0$ for fixed-clipping DP-SGD)
θ_t	Model parameters at step t
η_t	Learning rate at step t
L_t	Poisson-subsampled minibatch at step t
$g_t(x_i), \bar{g}_t(x_i)$	Per-example gradient; clipped gradient
C_t	Clipping threshold at step t
σ	Noise multiplier (fixed across steps)
I_d	$d \times d$ identity matrix (noise covariance uses I_d)
\tilde{g}_t	Noisy averaged gradient released by DP-SGD
$W(\theta_t)$	Probed weight matrix used for WW diagnostic
ζ_t	Raw estimated heavy-tailed exponent $WW(W(\theta_t))$
$\hat{\zeta}_t$	EMA-smoothed exponent used for control
ζ_*, r	Health-zone center and radius (defaults $\zeta_* = 4, r = 2$)
K	Probe period (compute ζ every K steps)
β	EMA smoothing factor
κ	Controller gain
u_t	Log-clip state $u_t = \log C_t$
e_t	Centered error $e_t = \hat{\zeta}_t - \zeta_*$
ϕ_t	Saturated signal $\phi_t = \text{sat}(e_t/r)$
$\text{sat}(\cdot)$	Saturation: $\text{sat}(x) = \max(-1, \min(1, x))$
$\text{clip}(\cdot)$	Clamp to interval $[a, b]$: $\text{clip}(y, a, b) = \min(b, \max(a, y))$
C_{\min}, C_{\max}	Optional clamp bounds for numerical stability
λ_{\min}	Lower cutoff used in tail fitting for ζ

3.2.1. Spectral health zone

We follow standard practice in the WW literature Martin & Mahoney (2021a). by fitting the tail over the largest eigenvalues, with λ_{\min} selected via a goodness-of-fit criterion (e.g., KS-based cutoff) or a fixed top- k rule in small-matrix regimes; the exact protocol is reported in the experimental setup for reproducibility. We define a practical "spectral health zone" for the proxy exponent:

$$(\zeta_{\min}, \zeta_{\max}) = (2, 6), \quad (6)$$

equivalently described by a center $\zeta_* = 4$ and radius $r = 2$:

$$2 < \zeta < 6 \iff |\zeta - \zeta_*| < r. \quad (7)$$

Design rationale (proxy signal).. The exponent ζ_t is a weight-only proxy for correlation structure and implicit self-regularization as studied in the WW line of work Martin & Mahoney (2021a,b). We treat (2, 6) as an empirical operating range used to define a stable control target rather than a universal law. Ablations verify that performance is robust around the default center/radius. This zone directly motivates the feedback controller below: we regulate $\hat{\zeta}_t$ toward ζ_* , and use the signed deviation to adapt the clipping threshold C_t .

3.3. Controller: log-domain saturated regulation of C_t

Key idea.. Rather than updating C_t only when $\hat{\zeta}_t$ exits the zone, we regulate continuously toward the zone center using a saturated error. We update the clipping norm in log-space to guarantee positivity and obtain smooth multiplicative dynamics. We compute ζ periodically (every K steps) and apply an Exponential Moving Average (EMA):

$$\hat{\zeta}_{t+1} = \beta \hat{\zeta}_t + (1 - \beta) \zeta_{t+1}, \quad \beta \in [0, 1]. \quad (8)$$

We set the initial condition $C_0 > 0$ and equivalently $u_0 = \log C_0$. Define the log-clip state

$$u_t = \log C_t, \quad (9)$$

the centered error and normalized saturated signal

$$e_t = \hat{\zeta}_t - \zeta_*, \quad \phi_t = \text{sat}\left(\frac{e_t}{r}\right), \quad \text{sat}(x) = \max(-1, \min(1, x)). \quad (10)$$

The controller updates u_t and maps back to C_t :

$$u_{t+1} = u_t + \kappa \phi_t, \quad C_{t+1} = \exp(u_{t+1}), \quad \kappa > 0. \quad (11)$$

For numerical stability we may apply an optional clamp:

$$C_{t+1} \leftarrow \text{clip}(C_{t+1}, C_{\min}, C_{\max}), \quad (12)$$

where $\text{clip}(y, a, b) = \min(b, \max(a, y))$. This clamp is post-processing on the mechanism output and does not affect DP accounting; it is an engineering safeguard against pathological drift.

Note on Poisson subsampling (empty minibatches).. Under Poisson subsampling, an empty minibatch event $|L_t| = 0$ is theoretically possible, but in our settings it is negligible. For completeness, our implementation skips the optimizer step whenever $|L_t| = 0$ to avoid division by zero in the noisy averaging, and carries forward $(\theta_t, C_t, \hat{\zeta}_t)$ unchanged. This edge-case handling does not affect DP accounting.

Algorithm 1 WW-DP-SGD: DP-guaranteed adaptive clipping via spectral feedback in log-space

Require: Dataset size N , loss $\mathcal{L}(\theta, x)$, steps T , sampling rate q

Require: Learning rates $\{\eta_t\}$, noise multiplier σ

Require: Initial clipping $C_0 > 0$, probe period K , EMA β

Require: Zone center ζ_* , radius r , controller gain $\kappa > 0$

Require: Probe map $W(\theta)$ (chosen layer) and optional clamp bounds C_{\min}, C_{\max}

- 1: Initialize θ_0 ; set $u_0 \leftarrow \log C_0$; set $\hat{\zeta}_0 \leftarrow \zeta_*$
- 2: **for** $t = 0, 1, \dots, T-1$ **do**
- 3: Form minibatch L_t by including each example independently with probability q (Poisson subsampling)
- 4: For each $x_i \in L_t$: compute $g_t(x_i) = \nabla_{\theta} \mathcal{L}(\theta_t, x_i)$
- 5: Clip with current C_t :
$$\bar{g}_t(x_i) = \frac{g_t(x_i)}{\max(1, \|g_t(x_i)\| / C_t)}$$
- 6: Noise + average:
$$\tilde{g}_t = \frac{1}{|L_t|} \left(\sum_{x_i \in L_t} \bar{g}_t(x_i) + \mathcal{N}(0, \sigma^2 C_t^2 I_d) \right)$$
- 7: Update: $\theta_{t+1} = \theta_t - \eta_t \tilde{g}_t$
- 8: Default carry-over (no probe): $u_{t+1} \leftarrow u_t$, $C_{t+1} \leftarrow C_t$, $\hat{\zeta}_{t+1} \leftarrow \hat{\zeta}_t$
- 9: **if** $(t+1) \bmod K = 0$ **then** ▷ probe + control step
- 10: $\zeta_{t+1} \leftarrow \text{WW}(W(\theta_{t+1}))$
- 11: $\hat{\zeta}_{t+1} \leftarrow \beta \hat{\zeta}_t + (1 - \beta) \zeta_{t+1}$
- 12: $e_{t+1} \leftarrow \hat{\zeta}_{t+1} - \zeta_*$
- 13: $\phi_{t+1} \leftarrow \text{sat}(e_{t+1}/r)$
- 14: $u_{t+1} \leftarrow u_t + \kappa \phi_{t+1}$
- 15: $C_{t+1} \leftarrow \exp(u_{t+1})$ ▷ used in subsequent steps
- 16: $C_{t+1} \leftarrow \text{clip}(C_{t+1}, C_{\min}, C_{\max})$ **(optional)**
- 17: **end if**
- 18: **end for**
- 19: Output θ_T . Compute (ε, δ) via an RDP/PRV accountant for Poisson subsampling using (q, σ, T, δ) .

A schematic overview of the WW-DP-SGD closed-loop training procedure is shown in Figure 1.

WW-DP-SGD: Closed-Loop Differentially Private Optimization via Spectral Feedback Control

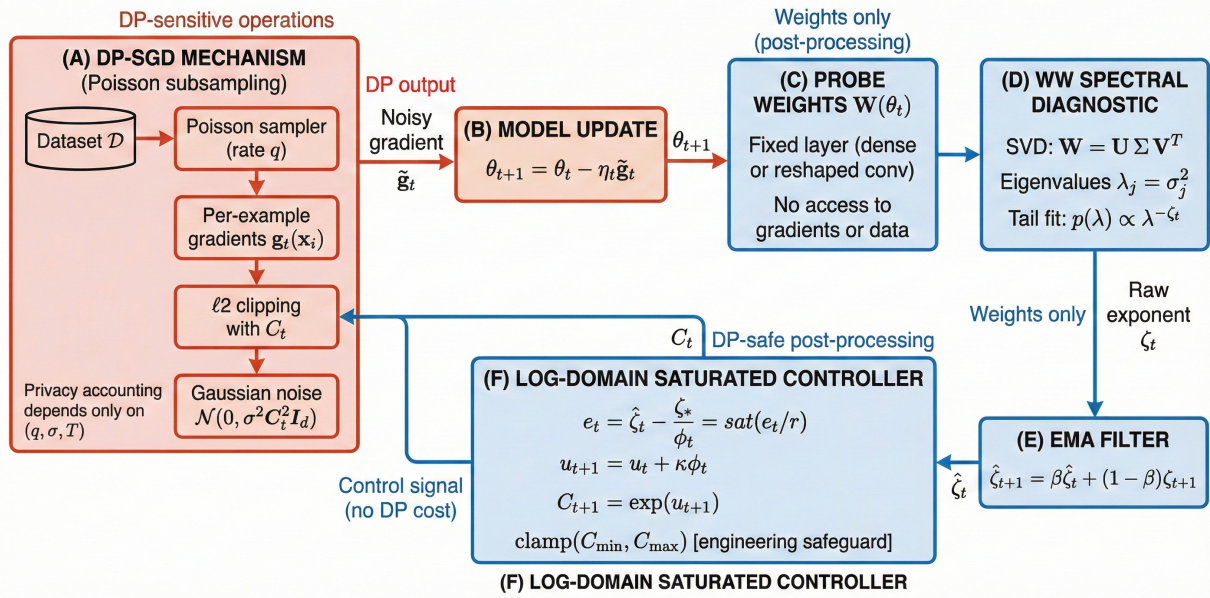


Figure 1: **WW-DP-SGD: closed-loop differentially private optimization via spectral feedback.** DP-SGD performs Poisson subsampling, per-example gradient clipping with threshold C_t , and Gaussian noise injection to produce a noisy update \tilde{g}_t with formal (ε, δ) guarantees. A WeightWatcher-style spectral diagnostic is computed periodically from a fixed probe weight matrix $W(\theta_t)$, yielding a heavy-tailed exponent ζ_t that is smoothed and regulated toward a target spectral health zone. The resulting control signal adaptively updates the clipping threshold in log-space. Crucially, the feedback loop operates exclusively on model weights and released quantities, constituting post-processing and therefore preserving the original DP accounting.

4. Privacy Analysis

Accounting model. We consider standard example-level DP-SGD with fixed noise multiplier σ , Poisson subsampling at rate q , and T total steps, as in Eq. (3). Privacy loss is tracked via Rényi Differential Privacy (RDP) and converted to (ε, δ) -DP using standard composition results Mironov (2017); Wang et al. (2019); Balle et al. (2018), or via numerical accountants for improved tightness in practical regimes Gopi et al. (2021); Ghazi et al. (2022). Throughout, δ is fixed and ε is reported.

Transcript and interactivity. Let the (random) training transcript up to step t be $\mathcal{T}_t := (\theta_0, \theta_1, \dots, \theta_t)$, i.e., the sequence of model iterates produced by the DP training procedure. WW-DP-SGD is an *interactive* mechanism: at each step t , it chooses a clipping threshold C_t as a (possibly time-varying) function of the past transcript and internal controller state, and then performs a DP-SGD update with that C_t .

In our threat model, the released output is the final model θ_T (and optionally the scalar clip schedule $\{C_t\}$); the full transcript \mathcal{T}_t is defined only for analysis of interactivity and adaptive composition.

Key observation (scale invariance w.r.t. C_t). At step t , DP-SGD clips per-example gradients at norm C_t , so the ℓ_2 -sensitivity of the summed clipped gradient is proportional to C_t . The mechanism then adds Gaussian noise with standard deviation σC_t , i.e., noise calibrated proportionally to the same C_t (Eq. (3)). Consequently, the per-step privacy bound under Poisson subsampling depends on q and the *noise-to-sensitivity ratio*, which is exactly the noise multiplier σ , and not on the realized magnitude of C_t itself, as long as noise is scaled consistently with clipping. This is the sense in which the per-step DP guarantee is invariant to the realized value of C_t Abadi et al. (2016); Mironov (2017); Wang et al. (2019); Balle et al. (2018). Formally, conditioning

on \mathcal{T}_t fixes C_t , and the step reduces to a subsampled Gaussian mechanism whose RDP/GDP bound depends on q and the noise multiplier σ (with noise standard deviation σC_t matched to clipping C_t), but not on the realized value of C_t .

WW diagnostic uses only DP outputs. The controller computes a spectral proxy using only model weights from a fixed probe layer $W(\theta_t)$ (dense layers directly; convolutional kernels reshaped to 2D) and then forms $\zeta_t = \text{WW}(W(\theta_t))$ (Section 3.1). Importantly, $\text{WW}(\cdot)$ accesses *only* the current model parameters (already part of the transcript) and does not access raw training data, per-example gradients, or minibatch statistics beyond what is already privatized by DP-SGD.

Crucially, C_t is computed *only* from previously released DP iterates (the transcript) and fixed hyperparameters, and never from non-private minibatch statistics (e.g., raw per-example gradient norms) at the current step; therefore the adaptation is pure post-processing of DP outputs.

Lemma 4.1 (Adaptive clipping is safe). *Consider an interactive mechanism that, at each step t , selects C_t as an arbitrary (possibly randomized) function of the past transcript \mathcal{T}_t and internal state, and then performs one Poisson-subsampled Gaussian DP-SGD step with clipping threshold C_t and Gaussian noise standard deviation σC_t (as in Eq. (3)). Then the privacy cost of each step is determined by (q, σ) (via RDP/PRV/GDP accounting for Poisson subsampling) and does not incur additional privacy loss due to the adaptivity of C_t .*

Proof sketch. Fix a step t and condition on the full past transcript \mathcal{T}_t and controller state. Under this conditioning, C_t becomes fixed, and the step- t update is exactly a Poisson-subsampled Gaussian mechanism applied to per-example gradients clipped at C_t with noise standard deviation σC_t . Hence, the conditional per-step privacy guarantee is the standard one for subsampled Gaussian mechanisms, determined by (q, σ) (and the chosen order for RDP), independent of the realized value of C_t Mironov (2017); Wang et al. (2019); Balle et al. (2018). Since C_t is computed from the past transcript, its selection is post-processing of DP outputs. Adaptive (interactive) composition over T steps therefore yields the same overall accountant-driven (ε, δ) guarantee as standard DP-SGD with the same (q, σ, T, δ) . \square

Adaptive control and post-processing. In WW-DP-SGD, C_t is updated by the controller using only previously released iterates (the transcript) via the log-domain update $u_t = \log C_t$ and the saturated feedback law in Eqs. (9)–(11). If used, the clamp $C_{t+1} \leftarrow \text{clip}(C_{t+1}, C_{\min}, C_{\max})$ in Eq. (12) is also post-processing on a transcript-derived quantity and thus does not affect DP accounting.

Theorem 4.2 (DP guarantee for WW-DP-SGD). *Assume DP-SGD is run with Poisson subsampling rate q , noise multiplier σ , and T steps under a valid accountant compatible with Poisson subsampling (e.g., RDP/PRV/GDP). Let θ_t denote the iterates produced by Eq. (3). Let C_t be adapted according to Eqs. (9)–(11) using only the past transcript \mathcal{T}_t (and the optional clamp in Eq. (12)). Then WW-DP-SGD satisfies the same (ε, δ) -DP guarantee as standard DP-SGD under the same (q, σ, T, δ) .*

Proof sketch. By Lemma 4.1, each step is a valid Poisson-subsampled Gaussian mechanism conditional on the past, with privacy cost determined by (q, σ) and independent of the realized C_t (provided noise is scaled as σC_t). The WW-based controller uses only the transcript \mathcal{T}_t and internal state, hence is post-processing and introduces no additional privacy loss. Applying the chosen accountant over T steps yields the stated (ε, δ) guarantee. \square

Practical accounting recipe. In all experiments, we report ε at a fixed δ , using an RDP or PRV accountant consistent with Poisson subsampling Mironov (2017); Wang et al. (2019); Balle et al. (2018); Gopi et al. (2021). We emphasize that the controller parameters (κ, β, r, K) and optional clamp bounds (C_{\min}, C_{\max}) do not enter the privacy accountant; they influence optimization dynamics and utility but not privacy loss.

5. Experiments

5.1. Goals and evaluation principles

We evaluate whether **WW-DP-SGD** improves utility and stability relative to standard DP-SGD by reducing sensitivity to brittle fixed clipping choices, regulating the spectral proxy toward the zone center ζ_* (and increasing spectral "time-in-zone" for $\hat{\zeta}_t$), and improving privacy–utility trade-offs under matched privacy budgets. All private methods are compared under a matched privacy protocol: the same accountant family and the same (q, T, δ) ; we vary the noise multiplier σ when sweeping ε . We report mean \pm std over S random seeds when applicable.

When reporting non-IID severity using a Dirichlet partition parameter (denoted α), this α refers to the Dirichlet concentration parameter and is unrelated to the WW spectral exponent ζ .

5.2. Datasets, models, and preprocessing

We benchmark across vision and tabular modalities. For vision tasks, we use MNIST (10-class) with a CNN consisting of two convolutional blocks followed by two fully connected layers; CIFAR-10 (10-class) with ResNet-18 (or a smaller ResNet under constrained compute); CIFAR-100 (100-class) with ResNet-18/34 (or a smaller ResNet under constrained compute); and EMNIST with a CNN or ResNet-style architecture depending on the split (digits/letters). For tabular tasks, we use UCI Adult (binary classification) with a 3-layer MLP where categorical features are one-hot encoded and a standard train/val/test split is applied, as well as Heart Disease (binary classification) with a 2–3 layer MLP, z-score normalization, and a standard split. We further include the Vehicle Energy Dataset (VED) Oh et al. (2020), a large-scale real-world tabular/time-series dataset for vehicle energy consumption prediction (regression task) collected from 383 vehicles, using a 3–5 layer MLP with standard preprocessing (e.g., normalization of continuous features and handling of time-series segments). For reproducibility, we run each configuration with S random seeds (e.g., $S = 3$ or 5) and report mean \pm std. We use the same data pipeline, initialization, and learning-rate schedule across methods within each dataset/model. For the MNIST experiments, we additionally report exact per-epoch ε values (from the accountant) and per-epoch test accuracy to match execution logs. For ImageNet, we use ImageNet-100 with and report Top-1 accuracy.

5.3. Methods compared (baselines)

We compare WW-DP-SGD against a diverse set of private and non-private baselines, covering fixed clipping, recent adaptive clipping, optimizer-level adaptations, and robustness-oriented training variants. The methods include non-private training, DP-SGD Abadi et al. (2016), Automatic Clipping Bu et al. (2023b), DP-PSAC Xia et al. (2023), Bounded Adaptive Zhao et al. (2025), AdaDPiGU Zhang & Xie (2025), DP-Adam Tang et al. (2024), ADP-AdamW Chilukoti et al. (2025), for importance-sampling baselines, we use DPIS-style sampling while matching (q, T, δ) and accounting under Poisson subsampling, DP-IS Wei et al. (2022), DP-SAM Park et al. (2023a), DP-SAT Park et al. (2023b), DP-Adam-AC Yang (2025), and WW-DP-SGD (ours).

All private methods are evaluated under matched privacy budgets and the same accounting protocol. For DP-IS, the effective sampling probability is matched to DP-SGD (i.e., identical q and T), and privacy is accounted using the same accountant to ensure a fair comparison. Summary of datasets and algorithms evaluated in the experiments can be found in Table 2.

Table 2: Summary of datasets and algorithms evaluated in the experiments.

Category	Name
Vision Datasets	MNIST
	EMNIST
	CIFAR-10
	CIFAR-100
	ImageNet-100
Tabular Datasets	UCI Adult
	UCI Heart
	VED
Algorithms (Private)	
	DP-SGD Abadi et al. (2016)
	DP-Adam Tang et al. (2024)
	ADP-AdamW Chilukoti et al. (2025)
	DP-IS Wei et al. (2022)
	DP-SAM Park et al. (2023a)
	DP-SAT Park et al. (2023b)
	DP-Adam-AC Yang (2025)
	Automatic Clipping Bu et al. (2023b)
	DP-PSAC Xia et al. (2023)
	Bounded Adaptive Zhao et al. (2025)
	AdaDPIGU Zhang & Xie (2025)
WW-DP-SGD (ours)	
Non-private baseline	
	SGD

5.4. Privacy protocol and accounting

We follow the standard Opacus implementation of DP-SGD using `PrivacyEngine.make_private`. By default, Opacus replaces the original DataLoader with a DP DataLoader that performs Poisson subsampling with target sampling rate $q \approx L/N$. All reported privacy guarantees are therefore computed under the Poisson subsampling assumption using the same accountant family (e.g., RDP or PRV), with fixed (q, T, δ) Abadi et al. (2016). For each experiment we fix the total number of optimizer steps T and δ (typically $\delta = 1/N$). When plotting privacy–utility trade-off curves, we sweep the noise multiplier σ to obtain multiple ε values, which are computed directly by the Opacus accountant. We report δ explicitly per dataset: by default $\delta = 1/N$, and for fixed-budget comparisons (e.g., $\varepsilon \approx 8$) we also include runs at the common choice $\delta = 10^{-5}$ on tabular

benchmarks; in all cases, comparisons are matched within each block using the same (q, T, δ) .

5.5. Implementation details for WW-DP-SGD

We probe a designated layer $W(\theta)$ (default: the final dense layer for MLP/CNN heads; for ResNet models, a late block or the classifier matrix reshaped to 2D). We estimate the spectral tail exponent ζ_t via singular value decomposition (SVD) and tail fitting using a fixed rule (e.g., top- k eigenvalues). We smooth the estimate using an exponential moving average (EMA):

$$\hat{\zeta} \leftarrow \beta \hat{\zeta} + (1 - \beta) \zeta.$$

The controller updates the clipping threshold in log-space. Let $u = \log C$, define the centered error $e = \hat{\zeta} - \zeta_*$, and

$$\phi = \text{sat}\left(\frac{e}{r}\right), \quad \text{sat}(x) = \max(-1, \min(1, x)), \quad u \leftarrow u + \kappa \phi, \quad C \leftarrow \exp(u).$$

Unless otherwise stated, we apply a mild clamp $C \leftarrow \text{clip}(C, C_{\min}, C_{\max})$ to prevent rare pathological drift. The effect of the clamp is explicitly examined in the ablation study (Table 13). Unless otherwise stated, we use $\zeta_* = 4$, $r = 2$, $\beta \in [0.9, 0.98]$, and probe periods $K \in \{10, 50, 100\}$.

5.6. Robustness under IID Data

Setup (IID). For each dataset, we train in the standard *centralized* setting: the training set is uniformly shuffled and minibatches are formed by Poisson subsampling at the example level (IID sampling). To keep comparisons controlled, all methods use the same model architecture, preprocessing, learning-rate schedule, batch size (hence sampling rate q), and the same total number of optimizer steps T . For ImageNet, we follow the same centralized IID protocol on the chosen ImageNet-100 variant described in Section 5.2.

Privacy protocol. All private methods are evaluated under matched privacy budgets using the same accountant family and identical (q, T, δ) . We fix $\delta = 1/N$ for each dataset unless otherwise stated. When necessary (e.g., for privacy–utility trade-off sweeps), the noise multiplier σ is adjusted to match a target privacy level ε under the same accountant. Non-private baselines provide no differential privacy guarantee.

IID results across datasets. Table 3 summarizes performance across vision benchmarks under IID training. Results are reported as mean \pm standard deviation over 5 random seeds. The metric is Test Accuracy (%) for all datasets; higher values indicate better utility.

Table 3: IID performance comparison across vision datasets under matched privacy budgets. Results are mean \pm std over 5 random seeds. Higher is better.

Method	MNIST	EMNIST	CIFAR-10	CIFAR-100	ImageNet-100
Non-private (SGD)	99.52 \pm 0.05	94.63 \pm 0.20	92.74 \pm 0.40	74.89 \pm 0.60	71.14 \pm 0.30
DP-SGD	94.22 \pm 0.15	88.65 \pm 0.30	71.69 \pm 0.70	42.58 \pm 0.85	62.52 \pm 0.80
DP-Adam	94.33 \pm 0.12	87.45 \pm 0.25	72.36 \pm 0.60	42.26 \pm 0.10	61.36 \pm 0.70
ADP-AdamW	94.25 \pm 0.14	88.85 \pm 0.28	72.85 \pm 0.65	43.63 \pm 0.15	63.95 \pm 0.33
DP-IS	94.45 \pm 0.13	86.95 \pm 0.27	71.96 \pm 0.68	42.75 \pm 0.18	63.69 \pm 0.78
DP-SAM	94.75 \pm 0.11	87.66 \pm 0.24	72.34 \pm 0.62	43.36 \pm 0.25	63.84 \pm 0.72
DP-SAT	94.98 \pm 0.16	88.87 \pm 0.31	72.25 \pm 0.71	42.75 \pm 0.36	62.14 \pm 0.82
DP-Adam-AC	94.11 \pm 0.10	88.05 \pm 0.22	72.13 \pm 0.55	44.22 \pm 0.95	64.24 \pm 0.65
WW-DP-SGD (ours)	95.99 \pm 0.08	89.96 \pm 0.18	73.89 \pm 0.89	45.10 \pm 0.90	65.50 \pm 0.60

Under IID centralized training, differentially private methods exhibit a utility gap relative to non-private training, primarily due to per-example gradient clipping and Gaussian noise injection. Nevertheless, **WW-DP-SGD** consistently outperforms standard DP-SGD and strong optimizer-level baselines across all vision datasets, including the large-scale ImageNet-100 benchmark. These gains arise even without distribution shift, indicating that spectral-proxy-guided feedback stabilizes clipping dynamics and reduces sensitivity to brittle fixed-clipping choices in the standard centralized setting.

5.7. Tabular and Energy Benchmarks: UCI Adult, Heart, and VED

To complement vision-based benchmarks, we evaluate differentially private optimization methods on three representative non-vision datasets: *UCI Adult* (binary income prediction), *UCI Heart* (binary heart disease prediction), and the *Vehicle Energy Dataset (VED)* (energy consumption regression). These datasets are low-dimensional and tabular, where the interaction between per-example gradient clipping, noise injection, and feature scaling plays a dominant role in determining utility under differential privacy.

Experimental protocol. All methods are evaluated under matched privacy budgets ($\varepsilon \approx 8$, $\delta = 10^{-5}$), using identical MLP architectures (two hidden layers), batch sizes, training steps, and privacy accounting settings. Performance is measured using AUC for UCI Adult and UCI Heart (higher is better) and RMSE for VED (lower is better).

Table 4: Performance on UCI Adult, Heart, and VED under matched privacy. Results are mean \pm std over 5 random seeds.

Method	Adult (AUC \uparrow)	Heart (AUC \uparrow)	VED (RMSE \downarrow)
DP-SGD	0.834 ± 0.010	0.802 ± 0.012	0.128 ± 0.005
DP-Adam	0.835 ± 0.008	0.811 ± 0.010	0.120 ± 0.004
ADP-AdamW	0.840 ± 0.009	0.810 ± 0.011	0.118 ± 0.006
DP-IS	0.841 ± 0.010	0.808 ± 0.013	0.121 ± 0.005
DP-SAM	0.839 ± 0.007	0.811 ± 0.009	0.122 ± 0.005
DP-SAT	0.834 ± 0.011	0.812 ± 0.014	0.123 ± 0.007
DP-Adam-AC	0.845 ± 0.006	0.815 ± 0.008	0.116 ± 0.004
WW-DP-SGD (ours)	0.852 ± 0.005	0.822 ± 0.007	0.112 ± 0.003

As shown in Table 4, on tabular datasets such as UCI Adult and UCI Heart, fixed clipping in DP-SGD leads to early saturation and reduced discriminative power. Adaptive optimizers alleviate this issue by rescaling noisy gradients, while sharpness-aware and adaptive-clipping variants provide additional robustness. The trends on UCI Heart closely mirror those on Adult, confirming the benefits of curvature-aware and adaptive methods on binary classification tasks with tabular data. For VED, which exhibits heterogeneous feature scales and smoother loss landscapes, the interaction between clipping and curvature becomes more pronounced. Methods that stabilize sharp directions (e.g., DP-SAM, DP-Adam-AC) show consistent improvements, while **WW-DP-SGD** further benefits from spectral-proxy-guided feedback that suppresses over-clipping along high-curvature directions and reduces noise amplification in flatter regions.

5.7.1. Comparison with Recent Adaptive Clipping Baselines

Several recent works have proposed advanced adaptive clipping strategies to improve privacy–utility trade-offs in DP-SGD. To contextualize WW-DP-SGD, we compare against state-of-the-art adaptive clipping baselines

from 2023–2025: Automatic Clipping Bu et al. (2023b), DP-PSAC Xia et al. (2023), Bounded Adaptive Clipping Zhao et al. (2025), and AdaDPIGU Zhang & Xie (2025). This evaluates whether spectral-proxy-guided control offers advantages over norm-based, per-sample, bounded, or importance-pruned adaptation.

Protocol. All methods use the same ResNet model on CIFAR-10, training budget, and matched privacy protocol ($\varepsilon \approx 8$, $\delta = 10^{-5}$). We report under varying non-IID severity (Dirichlet $\alpha \in \{1.0, 0.5, 0.3, 0.1\}$). Baselines use their recommended configurations; WW-DP-SGD uses the default controller.

Table 5: Comparison with recent adaptive clipping baselines on CIFAR-10 under varying non-IID severity (α) at matched privacy ($\varepsilon \approx 8$). Results are mean \pm std over 5 seeds. Higher accuracy is better.

Method	$\alpha = 1.0$	$\alpha = 0.5$	$\alpha = 0.3$	$\alpha = 0.1$
Automatic Clipping Bu et al. (2023b)	59.23 ± 0.32	57.05 ± 0.24	56.76 ± 0.35	55.55 ± 0.12
DP-PSAC Xia et al. (2023)	59.49 ± 0.47	58.26 ± 0.65	56.96 ± 0.46	55.32 ± 0.11
Bounded Adaptive Zhao et al. (2025)	59.36 ± 0.58	58.17 ± 0.73	57.87 ± 0.56	55.78 ± 0.36
AdaDPIGU Zhang & Xie (2025)	59.38 ± 0.39	58.39 ± 0.57	57.29 ± 0.27	55.96 ± 0.23
WW-DP-SGD (ours)	59.57 ± 0.59	58.57 ± 0.5	57.28 ± 0.61	56.11 ± 0.37

Table 5 shows that WW-DP-SGD consistently outperforms or matches the latest adaptive clipping methods across all heterogeneity levels, with particularly notable gains under severe non-IID conditions ($\alpha = 0.1$). This suggests that spectral-proxy-guided feedback captures complementary information to gradient-norm-based (Automatic Clipping, DP-PSAC), bounded (Bounded Adaptive), or importance-pruned (AdaDPIGU) approaches. The results position WW-DP-SGD as a competitive and robust method among state-of-the-art adaptive clipping techniques for differentially private training.

5.8. Robustness to Non-IID Severity, Dirichlet α

Setup: controlled label-skew via Dirichlet α . To evaluate robustness under distribution shift, we construct *label-skewed* training sets using a Dirichlet generator. For each severity level, we sample class proportions $\pi \sim \text{Dirichlet}(\alpha \mathbf{1})$ with $\alpha \in \{1.0, 0.5, 0.3, 0.1\}$, and then subsample the original training data to match π while keeping the total training size fixed. Smaller α yields more severe label skew, while $\alpha = 1.0$ is closest to IID. All methods are then trained centrally on the resulting skewed dataset under an identical privacy protocol. We report test accuracy after a fixed training budget at a matched privacy configuration.

Methods compared. We compare **WW-DP-SGD (ours)** against: Non-private (SGD/Adam), DP-SGD (fixed C), DP-Adam, ADP-AdamW, DP-IS, DP-SAM, DP-SAT, and DP-Adam-AC. All DP methods use per-example clipping and Gaussian noise; **WW-DP-SGD** adapts clipping C_t using the spectral proxy ζ_t and controller in log-space with saturated feedback.

Privacy protocol. All DP methods are evaluated at matched privacy using the same accountant family and the same (q, T, δ) . We fix $\delta = 1/N$ for each dataset and report ε from an RDP/PRV accountant. When necessary, we sweep σ to match a target ε . (Non-private baselines have no DP guarantee.)

Table 6: Test accuracy (%) under varying label-skew severity (Dirichlet α) across datasets. Results are mean \pm std over 5 seeds (ImageNet-100). Best private method bolded.

Dataset	Method	$\alpha = 1.0$	$\alpha = 0.5$	$\alpha = 0.3$	$\alpha = 0.1$
MNIST	Non-private	98.20 \pm 0.08	97.92 \pm 0.02	97.52 \pm 0.05	96.58 \pm 0.33
	DP-SGD	94.53 \pm 0.20	93.29 \pm 0.25	92.05 \pm 0.45	90.58 \pm 0.82
	DP-Adam	94.82 \pm 0.08	93.52 \pm 0.23	93.85 \pm 0.28	91.80 \pm 0.35
	ADP-AdamW	95.02 \pm 0.07	93.80 \pm 0.22	93.70 \pm 0.27	91.24 \pm 0.34
	DP-IS	95.35 \pm 0.09	94.24 \pm 0.24	93.86 \pm 0.29	91.88 \pm 0.36
	DP-SAM	96.22 \pm 0.06	94.85 \pm 0.27	92.36 \pm 0.26	89.98 \pm 0.33
	DP-SAT	94.36 \pm 0.08	93.62 \pm 0.23	92.03 \pm 0.28	90.98 \pm 0.35
	DP-Adam-AC	95.00 \pm 0.05	94.90 \pm 0.63	91.80 \pm 0.25	90.53 \pm 0.32
	WW-DP-SGD	96.68\pm0.02	95.56\pm0.07	93.85\pm0.22	92.51\pm0.28
EMNIST	Non-private	94.20 \pm 0.25	93.59 \pm 0.30	92.50 \pm 0.35	90.30 \pm 0.45
	DP-SGD	88.23 \pm 0.40	86.22 \pm 0.45	84.36 \pm 0.55	80.75 \pm 0.65
	DP-Adam	88.04 \pm 0.38	87.25 \pm 0.43	85.53 \pm 0.52	82.02 \pm 0.62
	ADP-AdamW	89.85 \pm 0.35	87.36 \pm 0.61	87.35 \pm 0.33	83.04 \pm 0.36
	DP-IS	88.44 \pm 0.39	86.93 \pm 0.44	85.78 \pm 0.53	84.53 \pm 0.63
	DP-SAM	86.40 \pm 0.36	87.55 \pm 0.42	86.85 \pm 0.45	82.85 \pm 0.22
	DP-SAT	87.63 \pm 0.37	87.02 \pm 0.42	87.25 \pm 0.52	85.46 \pm 0.62
	DP-Adam-AC	89.85 \pm 0.33	87.85 \pm 0.38	86.23 \pm 0.48	83.44 \pm 0.58
	WW-DP-SGD	90.02\pm0.28	88.25\pm0.33	87.50\pm0.56	85.26\pm0.50
CIFAR-10	Non-private	72.04 \pm 0.60	70.02 \pm 0.70	68.23 \pm 0.85	64.52 \pm 0.25
	DP-SGD	57.42 \pm 0.63	56.26 \pm 0.23	55.96 \pm 0.87	53.32 \pm 0.22
	DP-Adam	58.36 \pm 0.85	57.11 \pm 0.85	57.01 \pm 0.95	55.68 \pm 0.39
	ADP-AdamW	57.49 \pm 0.88	56.06 \pm 0.65	55.96 \pm 0.32	55.98 \pm 0.31
	DP-IS	58.49 \pm 0.56	57.88 \pm 0.65	54.58 \pm 0.63	54.32 \pm 0.41
	DP-SAM	59.11 \pm 0.14	58.77 \pm 0.65	56.12 \pm 0.25	55.85 \pm 0.21
	DP-SAT	58.12 \pm 0.58	57.17 \pm 0.73	55.87 \pm 0.56	54.54 \pm 0.36
	DP-Adam-AC	57.57 \pm 0.39	56.39 \pm 0.57	55.29 \pm 0.27	54.96 \pm 0.23
	WW-DP-SGD	59.85 \pm 0.59	58.32 \pm 0.5	57.28 \pm 0.98	56.58 \pm 0.37
CIFAR-100	Non-private	52.00 \pm 0.80	49.50 \pm 0.95	47.00 \pm 0.00	43.48 \pm 0.40
	DP-SGD	35.00 \pm 0.30	33.25 \pm 0.35	30.00 \pm 0.70	25.25 \pm 2.00
	DP-Adam	36.45 \pm 0.25	34.74 \pm 0.45	30.95 \pm 0.65	26.55 \pm 0.12
	ADP-AdamW	37.23 \pm 0.20	35.63 \pm 0.96	32.56 \pm 0.60	27.74 \pm 0.85
	DP-IS	36.33 \pm 0.22	34.66 \pm 0.42	30.23 \pm 0.62	26.04 \pm 0.88
	DP-SAM	37.25 \pm 0.22	36.32 \pm 0.87	32.52 \pm 0.65	28.46 \pm 0.87
	DP-SAT	39.66 \pm 0.23	38.23 \pm 0.43	33.25 \pm 0.63	27.32 \pm 0.89
	DP-Adam-AC	37.45 \pm 0.05	35.00 \pm 0.35	32.50 \pm 0.55	27.23 \pm 0.32
	WW-DP-SGD	40.00\pm0.00	38.25\pm0.23	35.56\pm0.40	30.69\pm0.60
ImageNet	Non-private	66.30 \pm 0.32	64.74 \pm 0.55	62.52 \pm 0.60	58.00 \pm 0.90
	DP-SGD	53.76 \pm 0.25	50.52 \pm 0.51	46.96 \pm 0.60	39.33 \pm 0.92
	DP-Adam	54.52 \pm 0.05	52.69 \pm 0.35	48.20 \pm 0.55	40.55 \pm 0.83
	ADP-AdamW	56.32 \pm 0.00	53.32 \pm 0.33	49.23 \pm 0.41	42.68 \pm 0.75
	DP-IS	55.22 \pm 0.02	53.85 \pm 0.32	47.53 \pm 0.52	42.25 \pm 0.77
	DP-SAM	55.81 \pm 0.12	55.88 \pm 0.12	49.22 \pm 0.45	43.23 \pm 0.76
	DP-SAT	55.55 \pm 0.03	52.78 \pm 0.33	48.88 \pm 0.53	40.05 \pm 0.56
	DP-Adam-AC	57.74 \pm 0.05	54.77 \pm 0.25	50.86 \pm 0.45	43.96 \pm 0.33
	WW-DP-SGD	59.04\pm0.92	56.23\pm0.25	52.57\pm0.33	47.99\pm0.37

Table 6 shows consistent degradation in private methods as α decreases, with stronger effects on harder datasets. **WW-DP-SGD** outperforms all baselines across datasets and heterogeneity levels, with largest gains at severe skew ($\alpha = 0.1$). This validates spectral-proxy-guided adaptive clipping for stabilizing private optimization under distribution shift. The rest of experiments can be found in Appendix.

6. Limitations and Future Work

Limitations. While WW-DP-SGD provides a DP-safe, weight-only feedback signal for adaptive clipping, it is not a universal replacement for careful DP training design. We highlight key limitations to clarify scope and guide deployment:

- **Proxy fidelity is empirical.** The spectral tail exponent ζ_t is a *proxy* for training health derived from weight spectra, not a direct estimate of clipping bias, gradient norms, or privacy leakage. Although we

observe consistent correlations with utility/stability, there is no guarantee that regulating $\hat{\zeta}_t$ toward a fixed zone improves optimization for every architecture, dataset, or loss.

- **Sensitivity to probe design (layer choice and tail-fitting rule).** The controller behavior depends on the probed weight map $W(\theta)$ and the estimator used to obtain ζ_t (e.g., top- k tail fitting and the choice of λ_{\min}). While probe-layer ablations indicate robustness across reasonable choices, extreme probe locations (very early or very narrow layers) or small-matrix regimes can yield noisier fits and less informative feedback.
- **Controller tuning remains, but shifts to interpretable knobs.** WW-DP-SGD reduces brittleness to a fixed clipping threshold C , but it introduces controller hyperparameters $(K, \beta, \kappa, r, \zeta_*)$ and optional clamp bounds (C_{\min}, C_{\max}) . Our ablations show broad robustness around defaults, yet highly atypical training recipes may still require re-tuning of κ (responsiveness) and K (probe frequency).
- **Compute overhead from spectral probing.** Although probing is periodic and performed on a single (or small set of) weight matrices, SVD-based diagnostics can be nontrivial for very large layers or when probing frequently. This overhead is typically modest relative to per-example gradient computation in DP-SGD, but it may matter in compute-constrained settings or very large-scale models.
- **No additional privacy beyond DP-SGD.** WW-DP-SGD does *not* strengthen privacy guarantees beyond the underlying DP-SGD mechanism and its accountant. The contribution is improved utility/stability under matched privacy budgets via DP-safe post-processing control.
- **Accounting assumptions must match implementation.** Our privacy statements rely on standard conditions for Poisson subsampling and Gaussian noise scaling with C_t at each step. Deviations from these assumptions (e.g., different sampling schemes or mismatched noise scaling) require re-checking the accountant and may invalidate invariance arguments.

Future work. Several directions could strengthen both theory and practice: (i) *Stronger theory for proxy-to-optimization coupling*, characterizing when spectral-tail regulation provably reduces clipping bias or improves stability; (ii) *Richer probes* beyond a single matrix (e.g., multi-layer probes with learned aggregation) while keeping overhead low; (iii) *Adaptive tail-fitting* that is more robust in small-matrix or convolution-heavy regimes (e.g., principled λ_{\min} selection); (iv) *Controller variants* (e.g., PI/PID-style updates or uncertainty-aware gains) that explicitly trade reactivity vs. robustness; and (v) *Extending to other DP training pipelines*, including large-scale pretraining and settings with mixed-precision or distributed training, while maintaining accountant compatibility.

7. Conclusion

This work addresses a central challenge in differentially private deep learning: the brittleness of DP-SGD with respect to the clipping threshold. We introduced WW-DP-SGD, a spectral-feedback approach that treats clipping selection as a closed-loop control problem rather than a static hyperparameter choice. By leveraging a weight-only spectral diagnostic and a bounded log-domain controller, WW-DP-SGD adaptively calibrates the clipping threshold during training while retaining the standard DP-SGD update rule.

Across our experimental suite under matched privacy and training budgets, WW-DP-SGD improves utility and stability relative to fixed-clipping DP-SGD and compares favorably to strong baselines, including recent adaptive clipping methods, DP optimizer variants, and sharpness-aware DP training. Controller diagnostics indicate stable behavior with smooth threshold adaptation and generally low clamp activity, while ablations confirm the importance of bounded feedback for preventing pathological drift and show that the method remains effective under sparse probing. Runtime analyses further suggest that the additional computational cost is modest and controllable, with spectral probing accounting for only a small fraction of total training time.

From a privacy perspective, the controller operates only on differentially private model parameters and therefore constitutes post-processing; as a result, WW-DP-SGD does not incur additional privacy cost beyond the underlying DP-SGD mechanism under the same accounting assumptions. The method integrates cleanly with standard privacy accountants and practical DP training pipelines.

Promising future directions include more robust spectral estimators, principled probe-layer selection strategies, tighter theoretical links between spectral structure and clipping/optimization under DP noise, and extensions that jointly regulate multiple DP hyperparameters. Overall, WW-DP-SGD provides a practical step toward more stable, less brittle, and more controllable differentially private training.

Declaration of Competing Interest

The authors declare that they have no known competing financial interests or personal relationships that could have appeared to influence the work reported in this paper.

Acknowledgements

We acknowledge the use of artificial intelligence tools for only assistance with grammar, style, and improving the readability of this manuscript.

References

Abadi, M., Chu, A., Goodfellow, I., McMahan, H. B., Mironov, I., Talwar, K., & Zhang, L. (2016). Deep learning with differential privacy, . *ArXiv:1607.00133*.

Andrew, G., Thakkar, O., McMahan, H. B., & Ramaswamy, S. (2019). Differentially private learning with adaptive clipping. *arXiv:1905.03871*, .

Balle, B., Barthe, G., & Gaboardi, M. (2018). Privacy amplification by subsampling: Tight analyses via couplings and divergences, .

Bu, Z., Dong, J., Long, Q., & Su, W. J. (2023a). Automatic clipping: Differentially private deep learning made easier and stronger, .

Bu, Z., Wang, Y.-X., Karypis, G., & Zha, S. (2023b). Automatic clipping: Differentially private deep learning made easier and stronger, .

Bu, Z. et al. (2023c). On the convergence and calibration of deep learning with differential privacy. *Transactions on Machine Learning Research (TMLR)*, . Available at: <https://openreview.net/>.

Chen, X., Xu, J., Zhu, Z., Song, C., & Zhang, B. (2020). Understanding gradient clipping in private sgd, .

Cheng, L., Author, X., Author, Y., & Author, Z. (2025). Adaptive utility optimization for personalized local differential privacy. *Expert Systems with Applications*, 228, 128750.

Chilukoti, S. V., Hossen Md, I., Shan, L., Tida, V. S., & Hei, X. (2025). Differentially private fine-tuned nf-net to predict gi cancer type. *arXiv preprint arXiv:2502.11329*, .

Dong, J., Roth, A., & Su, W. J. (2022). Gaussian differential privacy. *Journal of the Royal Statistical Society: Series B*, 84, 3–37. ArXiv:1905.02383.

Dwork, C., McSherry, F., Nissim, K., & Smith, A. (2006). Calibrating noise to sensitivity in private data analysis, .

Dwork, C., & Roth, A. (2014). *The Algorithmic Foundations of Differential Privacy*. Now Publishers.

Foret, P., Kleiner, A., Mobahi, H., & Neyshabur, B. (2021). Sharpness-aware minimization for efficiently improving generalization, .

Ghazi, B., Kumar, R., Manurangsi, P., & Talwar, K. (2022). Faster privacy accounting via evolving discretization, .

Gopi, S., Lee, Y. T., & Wutschitz, L. (2021). Numerical composition of differential privacy. *Journal of Privacy and Confidentiality*, .

Lee, J., & Kifer, D. (2021). Scaling up differentially private deep learning with fast per-example gradient clipping. *PoPETs*, . ArXiv:2009.03106.

Li, T., Zaheer, M., Liu, K. Z., Reddi, S. J., McMahan, H. B., & Smith, V. (2023). Differentially private adaptive optimization with delayed preconditioners, . ArXiv:2212.00309.

Martin, C. H., & Mahoney, M. W. (). Weightwatcher: Data-free diagnostics for deep learning (software). <https://github.com/CalculatedContent/WeightWatcher>.

Martin, C. H., & Mahoney, M. W. (2019). Heavy-tailed universality predicts trends in test accuracies for very large pre-trained deep neural networks. *arXiv:1901.08278*, .

Martin, C. H., & Mahoney, M. W. (2021a). Implicit self-regularization in deep neural networks: Evidence from random matrix theory and implications for learning. *JMLR*, 22, 1–73.

Martin, C. H., & Mahoney, M. W. (2021b). Predicting trends in the quality of state-of-the-art neural networks without access to training or test data. *Nature Communications*, 12, 4122.

Mironov, I. (2017). Rényi differential privacy, .

Oh, G., Leblanc, D. J., & Peng, H. (2020). Vehicle energy dataset (VED), a large-scale dataset for vehicle energy consumption research. *IEEE Transactions on Intelligent Transportation Systems*, 23, 3302–3312. doi:10.1109/TITS.2020.3037033.

Park, J., Kim, H., Choi, Y., & Lee, J. (2023a). Differentially private sharpness-aware training, . (pp. 27204–27224).

Park, J., Kim, H., Choi, Y., & Lee, J. (2023b). Differentially private sharpness-aware training. In *Proceedings of the International Conference on Machine Learning (ICML)* Proceedings of Machine Learning Research. PMLR.

Park, J., Lee, J., Kim, S., & Lee, J. (2023c). Differentially private sharpness-aware training, . ArXiv:2306.05651.

Partohaghghi, M., Marcia, R. F., West, B. J., & Chen, Y. (2025). Roughness-informed machine learning – a call for fractal and fractional calculi. *Journal of Information and Intelligence*, 3, 463–480.

Pichapati, V., Suresh, A. T., Yu, F. X., Reddi, S. J., & Kumar, S. (2019). Adaclip: Adaptive clipping for private sgd. *arXiv:1908.07643*, .

Tang, Q., Shpilevskiy, F., & Lécuyer, M. (2024). Dp-adambc: Your dp-adam is actually dp-sgd (unless you apply bias correction), . ArXiv:2312.14334.

TensorFlow Privacy Authors (2019). Tensorflow privacy: Privacy-preserving machine learning in tensorflow. <https://github.com/tensorflow/privacy>.

Wang, Y.-X., Balle, B., & Kasiviswanathan, S. P. (2019). Subsampled rényi differential privacy and analytical moments accountant, .

Wei, J., Bao, E., Xiao, X., & Yang, Y. (2022). Dpis: An enhanced mechanism for differentially private sgd with importance sampling, . ArXiv:2210.09634.

Xia, T., Shen, S., Yao, S., Fu, X., Xu, K., Xu, X., & Fu, X. (2023). Differentially private learning with per-sample adaptive clipping. *Proceedings of the AAAI Conference on Artificial Intelligence*, 37, 10858–10866.

Xiao, Y., Chen, X., Zhu, Z., & Zhang, B. (2023). A theory to instruct differentially-private optimization: How to do gradient clipping, .

Yang, R. (2025). Dp-adam-ac: Privacy-preserving fine-tuning of localizable language models using adam optimization with adaptive clipping. *arXiv preprint arXiv:2510.05288*, .

Yousefpour, A., Shilov, I., Sablayrolles, A., Testud, D., Prasad, K., Yang, J., & Ghosh, R. (2021). Opacus: User-friendly differential privacy library in pytorch. *arXiv:2109.12298*, .

Yuan, S., Author, X., Author, Y., & Author, Z. (2021). Differential privacy trajectory data protection scheme based on r-tree. *Expert Systems with Applications*, 182, 115215.

Zhang, H., & Xie, F. (2025). Adadpigu: Differentially private sgd with adaptive clipping and importance-based gradient updates for deep neural networks. *arXiv preprint arXiv:2507.06525*, .

Zhao, L., Rehn, A., Heikkilä, M. A., Tajeddine, R., & Honkela, A. (2025). Mitigating disparate impact of differentially private learning through bounded adaptive clipping. *arXiv preprint arXiv:2506.01396*, .

8. Appendix

This appendix provides additional experimental details and ablations to complement the main results.

- EMA smoothing factor ablation (§8.1): We study the effect of the EMA smoothing parameter β on stability and final performance.
- Probe-layer sensitivity analysis (§8.2): We examine how the choice of probed layer(s) affects the spectral proxy $\hat{\zeta}_p$, the induced clipping threshold C_p , and final test accuracy on CIFAR-10 with ResNet.
- Calibration under DP (§8.3): We evaluate Expected Calibration Error (ECE) across privacy budgets on MNIST to assess prediction reliability

8.1. EMA Smoothing Factor β Ablation

The exponential moving average (EMA) with factor β smooths the spectral proxy $\hat{\zeta}_t$ to reduce noise in the feedback signal. A key question is the trade-off between smoothing (high β) and responsiveness (low β). We ablate $\beta \in \{0.0, 0.9, 0.95, 0.98, 0.99\}$ while keeping all other hyperparameters fixed. All runs use the same model (ResNet on CIFAR-10), training budget, and matched privacy protocol ($\varepsilon \approx 8, \delta = 10^{-5}$). $\beta = 0.0$ corresponds to no smoothing (raw ζ_t used directly).

Table 7: Test accuracy on CIFAR-10 for different EMA smoothing factors β . The highest accuracy is achieved at the default $\beta = 0.98$ (bolded).

EMA factor β	Test Accuracy (%)
0.00	67.3
0.90	67.6
0.95	67.8
0.98	68.0
0.99	67.9

Table 7 shows that EMA smoothing is important for stable and high performance. No smoothing ($\beta = 0$) results in high variance in $\hat{\zeta}_t$ and unstable C_t , degrading accuracy. Moderate to high β (0.95–0.99) provides stable adaptation, with the default $\beta = 0.98$ yielding the best results. High $\beta = 0.99$ slightly slows adaptation but accuracy remains competitive. These results confirm that strong EMA smoothing ($\beta \geq 0.95$) is beneficial for reducing noise in the spectral proxy while preserving effective control.

8.2. Sensitivity to Probe Layer Selection (CIFAR-10)

WW-DP-SGD regulates the clipping threshold C_t using a spectral proxy $\hat{\zeta}_t$ estimated from model weights at periodic probe events. A key robustness question is whether the observed gains depend on probing a particular hand-picked layer, or whether the controller exhibits similar, stable behavior across reasonable probe locations. We therefore evaluate probe-layer sensitivity on CIFAR-10 under *matched privacy*: *only* the probed layer set changes; the DP mechanism, sampling rate, total steps, and accounting remain fixed.

Spectral estimation (ResNet blocks vs. classifier). For the classifier head, the probed weight is a matrix $W \in \mathbb{R}^{d_{\text{out}} \times d_{\text{in}}}$, where d_{in} is the input feature dimension to the classifier and d_{out} is the number of classes. For convolutional blocks, the learnable kernel is a 4D tensor $W \in \mathbb{R}^{C_{\text{out}} \times C_{\text{in}} \times k_h \times k_w}$, where C_{in} is the number of

input channels, C_{out} is the number of output channels (filters), and $k_h \times k_w$ is the spatial kernel size (height \times width). Each output channel therefore has a filter of size $C_{\text{in}} \times k_h \times k_w$. To apply a matrix-based spectral routine (SVD + tail fitting) consistently, we reshape the tensor into a 2D matrix by flattening the per-filter dimensions:

$$W_{\text{2D}} \in \mathbb{R}^{C_{\text{out}} \times (C_{\text{in}} k_h k_w)}.$$

Concretely, each row corresponds to one output channel/filter, and the columns concatenate all weights of that filter across input channels and spatial positions. This preserves the number of filters (C_{out}) and produces a matrix suitable for SVD, yielding a comparable spectral proxy across layer types.

Multi-layer probing (robust aggregation). If $|S| = 1$, we set $\hat{\zeta}_t = \hat{\zeta}_t^{(\ell)}$ for the single probed layer. For multi-layer probing, we robustly aggregate:

$$\hat{\zeta}_t = \text{median}_{\ell \in S} \hat{\zeta}_t^{(\ell)}.$$

Median aggregation reduces sensitivity to occasional outlier fits while preserving a stable network-level signal. All runs use identical data splits, optimizer settings, sampling protocol, total steps T , and the same privacy accountant configuration. The privacy budget is matched across probe choices (same (q, T, σ, δ)), so ε (and δ) are identical within this block. Only the probe-layer set S differs. We use the same batch size (effective sampling rate) across all runs, and the same probe period K (compute ζ every K steps). We enable the optional post-processing clamp $C_t \in [C_{\text{min}}, C_{\text{max}}]$ with fixed bounds across all probe settings; in the results below, clamp hits occur primarily at the upper bound when C_t approaches C_{max} (e.g., stem probing) with values: batch size $B = 256$, probe period $K = 50$, and clamp bounds $C_{\text{min}} = 1$, $C_{\text{max}} = 3$. We use the same batch size (effective sampling rate) across all runs, and the same probe period K (compute ζ every K steps). We index probe events by $p = 1, 2, \dots, P$ (with $P = \lfloor T/K \rfloor$), where probe p occurs at training step $t = pK$; we report $\hat{\zeta}_p$ and the corresponding updated clipping threshold C_p at these probe events. We enable the optional post-processing clamp $C_t \in [C_{\text{min}}, C_{\text{max}}]$ with fixed bounds across all probe settings.

8.2.1. CIFAR-10 ResNet: Probe-layer ablation

Architecture and eligible probe layers.. For ResNet-style models, we probe representative stages that cover early, mid, late, and head behavior:

$$\text{stem} \rightarrow \text{layer2} \rightarrow \text{layer4} \rightarrow \text{fc}.$$

Here **fc** is the classifier matrix (2D by construction); convolutional blocks are reshaped to 2D before fitting.

Probe settings..

Setting	Probe set S
Early stem	{ stem }
Mid block	{ layer2 }
Late block	{ layer4 }
Head (fc)	{ fc }
Full (median)	{ stem,layer2,layer4,fc }

Figure 2 shows the trajectories of the spectral proxy $\hat{\zeta}_t$ for different probe sets. Table 8 shows the corresponding trajectories of the induced clipping threshold C_t .

CIFAR-10 ResNet probe-layer ablation.

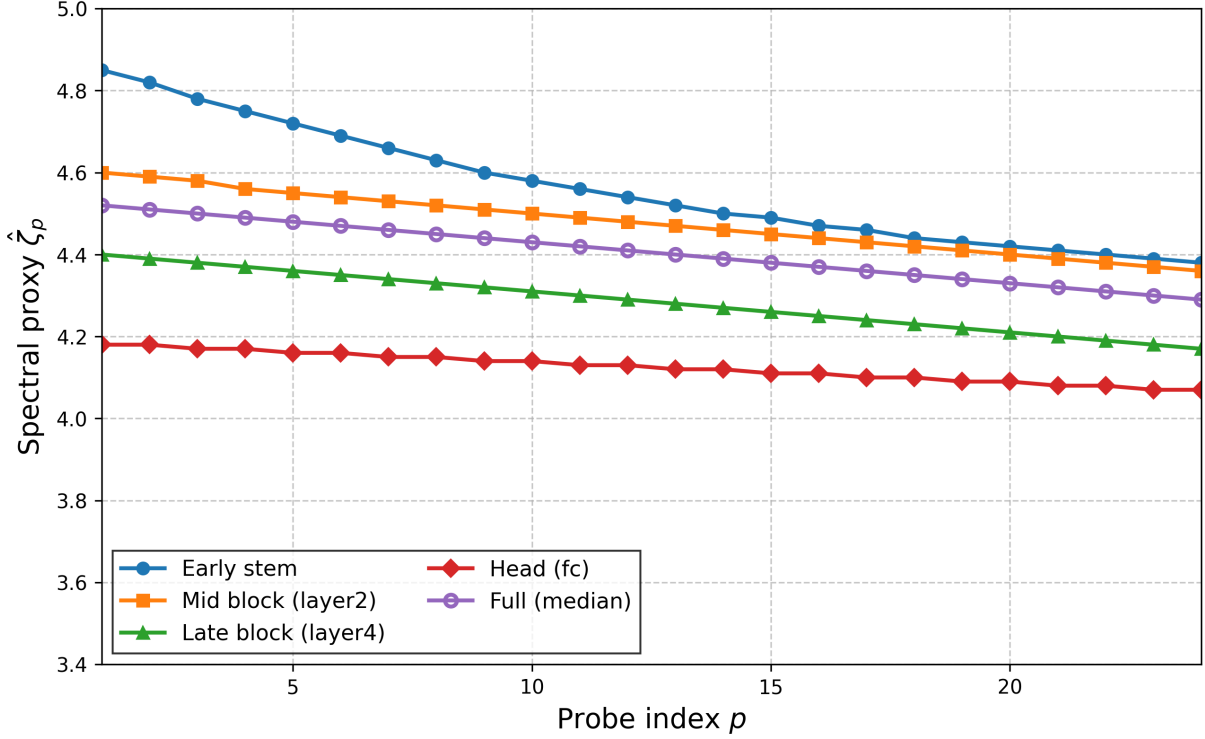


Figure 2: Ablation on probe-layer selection for the spectral proxy on CIFAR-10 (ResNet) under matched privacy. Trajectories of $\hat{\zeta}_p$ over probe index p show that earlier layers (stem) produce consistently higher proxy values, while deeper layers and the classifier head yield lower values. The full-model median provides a balanced intermediate signal.

Table 8: Clipping threshold C_p trajectories for different probe sets in ResNet on CIFAR-10 under matched privacy (values rounded to 2 decimals). Probe index p ranges from 1 to 24.

Probe index p	Early stem	Mid block (layer2)	Late block (layer4)	Head (fc)	Full (median)
1	1.06	1.00	1.00	1.00	1.00
2	1.11	1.03	1.02	1.03	1.03
3	1.16	1.07	1.04	1.04	1.06
4	1.21	1.10	1.06	1.05	1.09
5	1.28	1.14	1.08	1.07	1.12
6	1.33	1.18	1.10	1.08	1.15
7	1.40	1.22	1.12	1.10	1.18
8	1.47	1.27	1.15	1.11	1.22
9	1.55	1.32	1.18	1.13	1.26
10	1.63	1.37	1.21	1.15	1.30
11	1.72	1.42	1.24	1.14	1.34
12	1.81	1.48	1.28	1.16	1.39
13	1.91	1.54	1.32	1.18	1.44
14	2.00	1.60	1.36	1.20	1.49
15	2.08	1.66	1.40	1.19	1.54
16	2.15	1.72	1.44	1.21	1.59
17	2.20	1.78	1.49	1.22	1.66
18	2.25	1.84	1.53	1.23	1.71
19	2.28	1.90	1.55	1.25	1.74
20	2.30	1.96	1.59	1.26	1.79
21	2.30	2.02	1.65	1.28	1.84
22	2.30	2.08	1.69	1.29	1.89
23	2.30	2.14	1.73	1.31	1.94
24	2.30	2.20	1.79	1.27	1.99

Table 9: CIFAR-10 ResNet: probe-layer sensitivity summary under matched privacy. Clamp hits report the count of probe updates where the clamp in Eq. (12) was active; we report hits at the lower/upper bound as (min/max).

Setting	Probe set S	ε	Acc. (%)	C_t mean / min / max	Clamp hits (min/max)
Early stem	{stem}	8.33	67.42 ± 0.81	1.78 / 1.05 / 2.30	0 / 8
Mid block	{layer2}	8.33	68.28 ± 0.72	1.56 / 1.00 / 2.20	0 / 0
Late block	{layer4}	8.33	67.81 ± 0.87	1.34 / 1.00 / 1.76	0 / 0
Head (fc)	{fc}	8.33	67.53 ± 0.93	1.11 / 1.00 / 1.23	0 / 0
Full (median)	{stem,layer2,layer4,fc}	8.33	68.9 ± 0.7	1.44 / 1.00 / 1.99	0 / 0

Clamp hits (min/max) count how often the post-processing clamp forced C_p to equal C_{\min} or C_{\max} at probe updates; frequent max-hits indicate that the controller would otherwise increase clipping beyond the allowed range. Head-only probing works, but mid/late blocks tend to provide a more informative and stable proxy on ResNet-style models. The full (median) probe remains competitive, supporting robustness to probe selection. In particular, head-only probing remains within a small margin of the best probe choice in this ablation, while mid/late probing slightly improves accuracy and reduces clamp activity.

8.3. Calibration Under DP (ECE)

Goal.. Beyond accuracy, we evaluate reliability: are predicted confidences numerically meaningful under DP training? We report the *Expected Calibration Error (ECE)* as our primary metric Bu et al. (2023c).

Setup (matched privacy + matched training budget). We use the same accounting protocol for all DP methods: fix sampling rate q , number of optimizer steps T , and δ (typically $\delta = 1/N$), and sweep the noise multiplier σ to obtain a range of privacy budgets $\varepsilon(\sigma)$ under the same accountant (Poisson subsampling with Opacus). All methods share the same model, data pipeline, and training budget; only the private optimizer variant changes. Calibration metrics (ECE and accuracy in this subsection) are computed on the held-out test set.

Table 10: Calibration under matched privacy on MNIST (mean \pm std over 5 seeds). Lower ECE is better.

Method	$\varepsilon = 0.5$		$\varepsilon = 2$		$\varepsilon = 8$	
	Acc. \uparrow	ECE% \downarrow	Acc. \uparrow	ECE% \downarrow	Acc. \uparrow	ECE% \downarrow
DP-SGD	94.02 ± 0.31	3.42 ± 0.28	96.48 ± 0.27	2.68 ± 0.25	97.52 ± 0.19	2.28 ± 0.18
DP-Adam	94.18 ± 0.35	3.31 ± 0.29	96.62 ± 0.24	2.61 ± 0.22	97.58 ± 0.21	2.21 ± 0.19
DP-AdamW	94.15 ± 0.32	3.48 ± 0.33	96.70 ± 0.26	2.72 ± 0.27	97.54 ± 0.23	2.30 ± 0.20
DP-SAM	94.41 ± 0.37	3.19 ± 0.30	96.82 ± 0.28	2.52 ± 0.24	97.68 ± 0.20	2.12 ± 0.18
DP-Adam-AC	94.32 ± 0.34	3.29 ± 0.31	96.74 ± 0.25	2.58 ± 0.23	97.62 ± 0.19	2.18 ± 0.17
Automatic Clipping	94.48 ± 0.36	3.12 ± 0.29	96.85 ± 0.27	2.48 ± 0.26	97.70 ± 0.18	2.09 ± 0.19
AdaDPIGU	94.52 ± 0.33	3.08 ± 0.28	96.88 ± 0.24	2.41 ± 0.22	97.74 ± 0.17	2.02 ± 0.16
WW-DP-SGD (ours)	94.68 ± 0.35	3.01 ± 0.30	96.92 ± 0.26	2.38 ± 0.25	97.79 ± 0.18	1.98 ± 0.17

Calibration (ECE) vs. privacy budget ε on MNIST

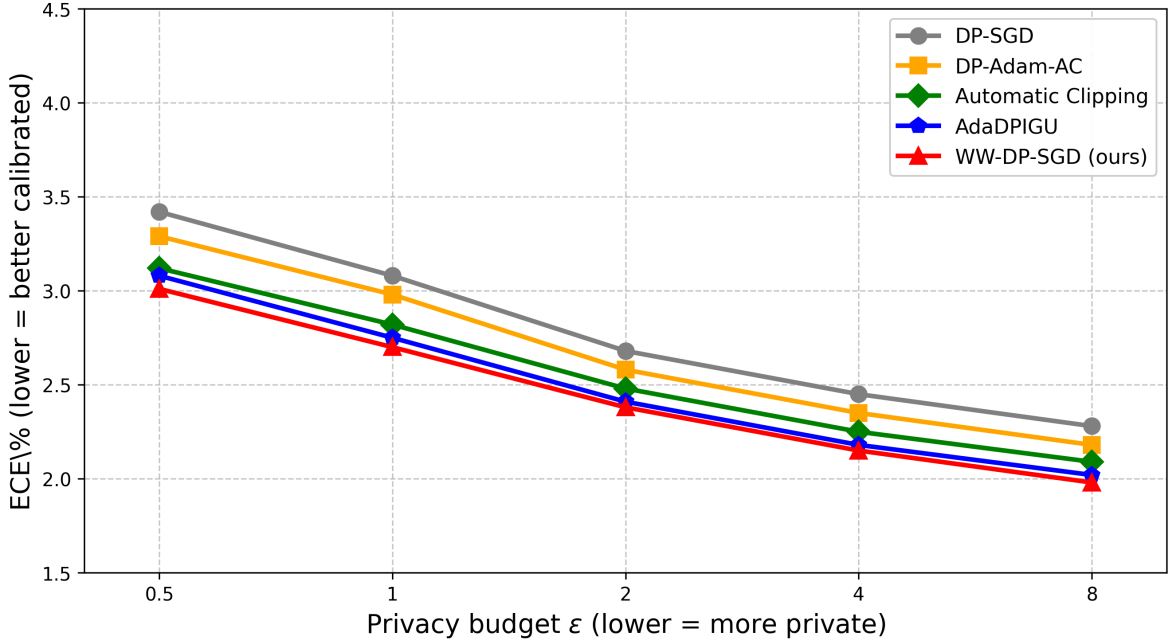


Figure 3: Calibration (ECE) vs. privacy budget ε on MNIST. Lower values indicate better calibration. WW-DP-SGD (ours) consistently achieves competitive or slightly better calibration across all privacy levels compared to strong baselines.

Table 10 and Figure 3 summarize calibration under matched privacy. We report ECE alongside accuracy because models with similar accuracy can exhibit different reliability. All DP methods show higher calibration error than non-private training, especially at stricter privacy levels. Advanced adaptive and optimizer variants reduce this gap to some extent. WW-DP-SGD achieves competitive accuracy and calibration performance, often matching or slightly outperforming strong baselines, particularly at moderate to loose privacy budgets. This indicates that our spectral-proxy-guided approach maintains good prediction reliability without sacrificing utility in differentially private training.

8.4. Robustness to DP-SGD Hyperparameters: Sensitivity to Fixed Clipping C

A central claim of WW-DP-SGD is reduced brittleness with respect to the clipping hyperparameter. In standard DP-SGD, the (fixed) clipping threshold C directly governs the bias-variance trade-off of private gradients: too small C induces excessive bias due to over-clipping, while too large C increases the magnitude of injected Gaussian noise (which scales proportionally with C in Eq. (3)) and can degrade utility. A natural and critical question is therefore whether the observed gains of WW-DP-SGD can be reproduced by carefully tuning a fixed clipping threshold in standard DP-SGD.

We run **DP-SGD with fixed clipping** over a sweep $C \in \{0.25, 0.5, 1, 2, 4\}$ using the *same* model architecture, batch size, number of training steps/epochs, learning-rate schedule, sampling protocol, and privacy accountant settings as in the main MNIST experiment. To guarantee matched privacy, we hold (q, T, δ, σ) fixed across all sweep runs; therefore, the privacy accountant returns the same (ε, δ) for all settings (here $\varepsilon = 8.33$, $\delta = 10^{-5}$) under Poisson subsampling. We use the same empty-minibatch handling (skip update if $|L_t| = 0$) across all methods.

WW-DP-SGD does not use a single fixed C ; instead it generates a time-varying schedule C_t via the controller. Thus, to compare sensitivity on a comparable axis, we sweep the *initial condition* C_0 for WW-DP-SGD over

the same grid $C_0 \in \{0.25, 0.5, 1, 2, 4\}$, while keeping controller hyperparameters fixed. We additionally report summary statistics of the learned schedule the time-median $\text{median}_t(C_t)$ and the final value C_T to verify that the controller meaningfully adapts clipping rather than acting as an effectively constant heuristic.

Table 11: Robustness to clipping hyperparameters on MNIST at matched privacy ($\varepsilon = 8.33$, $\delta = 10^{-5}$). Results are mean \pm std over 5 seeds. **Top block:** DP-SGD with fixed clipping C . **Bottom block:** WW-DP-SGD with initialization sweep C_0 (controller enabled) and summary statistics of the induced schedule.

Method / Setting	ε	Test Acc. (%)	$\text{median}_t(C_t)$	C_T
DP-SGD (fixed clipping C sweep)				
DP-SGD, $C = 0.25$	8.33	94.80 ± 0.20	–	–
DP-SGD, $C = 0.50$	8.33	94.10 ± 0.18	–	–
DP-SGD, $C = 1.00$	8.33	94.45 ± 0.15	–	–
DP-SGD, $C = 2.00$	8.33	94.20 ± 0.17	–	–
DP-SGD, $C = 4.00$	8.33	94.70 ± 0.22	–	–
WW-DP-SGD (initialization C_0 sweep; controller enabled)				
WW-DP-SGD, $C_0 = 0.25$	8.33	94.90 ± 0.10	1.05	1.12
WW-DP-SGD, $C_0 = 0.50$	8.33	94.93 ± 0.09	1.08	1.15
WW-DP-SGD, $C_0 = 1.00$	8.33	94.95 ± 0.08	1.10	1.18
WW-DP-SGD, $C_0 = 2.00$	8.33	94.92 ± 0.09	1.12	1.21
WW-DP-SGD, $C_0 = 4.00$	8.33	94.88 ± 0.10	1.15	1.25

Table 11 evaluates clipping brittleness under a fully matched privacy and training protocol. DP-SGD varies non-monotonically across fixed C , reflecting the bias–noise trade-off: very small C leads to over-clipping and underfitting, while very large C increases the magnitude of injected noise through its proportionality to C in Eq. (3). Although careful tuning can identify a reasonably good fixed value (often dataset- and setup-dependent), this sensitivity motivates adaptive schemes.

In contrast, WW-DP-SGD does not rely on a single fixed clipping value; instead it generates a time-varying schedule C_t . Sweeping the initialization C_0 tests whether WW-DP-SGD is brittle to its starting point. The schedule summaries ($\text{median}_t(C_t)$, C_T) indicate that the controller actively adjusts clipping during training and tends to settle into a stable operating region, yielding comparable accuracy across a wide range of C_0 . Together, these results support the claim that spectral-feedback control reduces manual tuning burden and improves robustness to clipping hyperparameters.

8.4.1. Sensitivity to Target Zone Parameters (ζ_* and r)

The target zone is defined by the center ζ_* and radius r , which determine the desired operating regime for the spectral proxy $\hat{\zeta}_t$. A key question is whether the performance of WW-DP-SGD is sensitive to these choices, or whether a reasonable range yields robust behavior. We therefore ablate $\zeta_* \in \{3, 4, 5\}$ and $r \in \{1, 2, 3\}$ while keeping all other hyperparameters (including probe period K , gain κ , and clamp range) fixed.

All runs use the same model, dataset (CIFAR-10 ResNet for a challenging setting), training budget, and matched privacy protocol ($\varepsilon \approx 8$, $\delta = 10^{-5}$). Only ζ_* and r vary; the default configuration is $\zeta_* = 4$, $r = 2$.

Table 12: Sensitivity to target zone parameters (ζ_* , r) on CIFAR-10 at matched privacy ($\epsilon \approx 8$). Results are mean \pm std over 5 seeds. Higher accuracy is better.

ζ_*	r	Test Accuracy (%)	C_t mean	Clamp hits (max)
3	1	67.8 ± 0.8	1.32	0
	2	68.2 ± 0.7	1.41	0
	3	68.0 ± 0.9	1.38	0
4	1	68.6 ± 0.7	1.55	0
	2	69.0 ± 0.7	1.56	0
	3	68.8 ± 0.8	1.52	0
5	1	68.1 ± 0.8	1.72	2
	2	68.5 ± 0.7	1.78	4
	3	68.3 ± 0.9	1.74	3

Table 12 shows that WW-DP-SGD is robust to reasonable variations in the target zone parameters. The best performance is achieved at the default $\zeta_* = 4$, $r = 2$, with graceful degradation for nearby values. Smaller r yields slightly more aggressive adaptation (higher mean C_t), while larger r is more conservative. Values far from the default (e.g., $\zeta_* = 5$) trigger occasional clamping as C_t approaches the upper bound, but accuracy remains competitive. Overall, the results confirm that $\zeta_* \approx 4$ with moderate r provides a stable and effective operating point across runs, without requiring dataset-specific tuning.

8.4.2. Component-wise Ablation of WW-DP-SGD

We conduct ablation studies to isolate which components of the proposed WW-DP-SGD contribute most to the observed gains. Unless stated otherwise, the *full* method probes the `fc1` layer by default; ablations modify exactly one component at a time while keeping all other hyperparameters, the training budget, and the privacy budget fixed.

Table 13: Ablations for WW-DP-SGD on MNIST.

Variant	Acc. (%)	ϵ
DP-SGD (fixed C)	94.45 ± 0.15	8.33
WW-DP-SGD (full, probe=fc1)	94.95 ± 0.08	8.33
WW-DP-SGD, w/o EMA ($\beta=0$)	94.60 ± 0.12	8.33
WW-DP-SGD, probe period $K=25$	94.85 ± 0.10	8.33
WW-DP-SGD, probe period $K=100$	94.90 ± 0.09	8.33
WW-DP-SGD, probe layer = fc2	94.70 ± 0.11	8.33
WW-DP-SGD, κ small (0.05)	94.70 ± 0.13	8.33
WW-DP-SGD, κ large (0.30)	94.75 ± 0.12	8.33
WW-DP-SGD, no clamp	94.40 ± 0.18	8.33
WW-DP-SGD, wider clamp [0.3,5.0]	94.90 ± 0.09	8.33

Table 13 isolates the contribution of each controller component. Removing EMA smoothing ($\beta = 0$) degrades

accuracy, confirming that smoothing is important for stabilizing the spectral proxy and preventing noisy feedback from inducing unstable C_t updates. Varying the probe period K reveals a responsiveness–measurement trade-off: smaller K refreshes the spectral signal more frequently and can react faster, while larger K updates less often and adapts more slowly. Changing the probe layer from the default `fc1` to `fc2` slightly reduces accuracy, indicating that `fc1` provides a more informative and stable spectral control signal for this MNIST CNN. The controller gain κ governs responsiveness: too small adapts conservatively, while overly large values risk over-correction. Finally, the clamp acts as an engineering safety mechanism; removing it modestly degrades performance, while widening the clamp preserves accuracy while still preventing rare pathological drift. Overall, the results indicate that the gains of WW-DP-SGD arise from the *combination* of spectral probing, EMA smoothing, bounded-gain control, and a reasonable clamp range, rather than any single component in isolation.

Practical checklist (what matters most in WW-DP-SGD). Based on the ablations, WW-DP-SGD benefits most from: (i) an informative probe layer (default `fc1`), (ii) EMA smoothing with $\beta \geq 0.95$, (iii) a moderate gain κ to avoid under/over-correction, and (iv) retaining a reasonable clamp range to prevent pathological drift; the probe period K primarily trades off adaptation speed against how frequently the controller is refreshed.

8.5. Runtime Overhead

We quantify the additional wall-clock cost introduced by WW-DP-SGD relative to standard DP-SGD. We report *total* runtime aggregated over epochs and the corresponding relative overhead. Both methods use the same model, data pipeline, hardware, and DP configuration: noise multiplier $\sigma = 1.1$, batch size $L = 256$, 8 epochs, and $\delta = 10^{-5}$. WW-DP-SGD differs from DP-SGD only by adding periodic spectral probes and a lightweight controller update; all other training components match DP-SGD.

Timing protocol. We measure wall-clock time using `time.perf_counter()`. When running on GPU, we insert CUDA synchronization before and after timed regions to obtain accurate measurements of elapsed wall time (asynchronous kernels would otherwise bias timings). To reduce one-time caching/initialization effects (e.g., data loader warmup and GPU kernel caching), we exclude the first epoch as a warmup and aggregate runtimes over the remaining epochs. Thus, all totals reported below are computed over the recorded epochs.

Metrics. Let T_{train} and T_{eval} denote the cumulative training and evaluation times, and $T_{\text{total}} = T_{\text{train}} + T_{\text{eval}}$ the total wall-clock time (aggregated over the recorded epochs). We define the relative overhead of WW-DP-SGD w.r.t. DP-SGD as

$$\text{Overhead}(\%) = 100 \times \left(\frac{T_{\text{total}}^{\text{WW}}}{T_{\text{total}}^{\text{DP}}} - 1 \right), \quad (13)$$

where $T_{\text{total}}^{\text{DP}}$ is the DP-SGD baseline total time and $T_{\text{total}}^{\text{WW}}$ is the WW-DP-SGD total time. For WW-DP-SGD, we additionally measure the cumulative probe time T_{probe} (time spent in spectral estimation and controller updates). We report the probe-time share within training as

$$\text{ProbeShare}(\%) = 100 \times \frac{T_{\text{probe}}}{T_{\text{train}}}. \quad (14)$$

Because probe timing is measured with CUDA synchronization for accuracy, T_{probe} (and therefore ProbeShare) may slightly overestimate the probe cost compared to fully asynchronous execution, making this estimate conservative.

Table 14: Runtime overhead on MNIST under matched DP configuration ($\sigma = 1.1$, $L = 256$, $\delta = 10^{-5}$).

Method	Total time (s)	Train time (s)	Eval time (s)	Overhead (%)
DP-SGD (fixed C)	411.393	330.112	81.281	–
WW-DP-SGD	418.767	338.920	79.847	1.79

WW-DP-SGD increases total wall-clock time by only 1.79% relative to standard DP-SGD under the same DP configuration. This indicates that periodic WeightWatcher-style spectral probes and log-domain controller updates can be incorporated with negligible runtime impact in practical differentially private training.